AIAA JOURNAL
Vol. 39, No. 4, April 2001

# Sidejet Aerodynamic Interaction Effects of the Missile

Kousuke Kikumoto* and Etsuroh Sentoh†
*Japan Defense Agency, Tokyo 190-8533, Japan*
Hideki Tanaka‡
*IHI Aerospace Company, Ltd., Gunma 370-2398, Japan*
and
Tatsuo Takahashi§
*Kawasaki Heavy Industries, Ltd., Gifu 504-8710, Japan*

**The side thruster is a highly responsive means for attitude control of missiles. The sidejet force is influenced by the interaction of the sidejet with the external airflow. The sidejet aerodynamic interaction effects were analyzed from following two viewpoints: 1) the pressure field in the vicinity of the sidejet and 2) the force acting on the missile. Technical data of sidejet aerodynamic interaction effects were obtained by means of flight tests of missiles that were equipped with four impulse side thrusters that were small-size, rapidly burning solid-propellant rocket motors. The data agree with computational fluid dynamics analyses and wind-tunnel tests.**

## Nomenclature

| | | |
|---|---|---|
| $d_j$ | = | nozzle exit diameter, m |
| $\boldsymbol{F}$ | = | force, N |
| $I_y$ | = | inertia moment, kg · m$^2$ |
| $I_0$ | = | impulse of thruster, N · s |
| $l$ | = | length between thruster and c.g., m |
| $\ell$ | = | length from thruster nozzle, m |
| $\boldsymbol{M}$ | = | moment, N · m |
| $M$ | = | Mach number |
| $m$ | = | mass of missile, kg |
| $P$ | = | pressure, N/m$^2$ |
| $q$ | = | angular velocity around yaw axis, deg/s |
| SSM | = | static stability margin, m |
| $T$ | = | temperature, K |
| $V$ | = | velocity, m/s |
| $x, y, z$ | = | coordinates in body axis, m |
| $\gamma$ | = | flight-path angle, deg |
| $\kappa$ | = | gas specific heat ratio |
| $\rho$ | = | density, kg/m$^3$ |

*Subscripts*

| | | |
|---|---|---|
| $j$ | = | jet |
| max | = | maximum |
| $u$ | = | uniform flow |
| 0 | = | stagnation conditions |

*Superscript*

| | | |
|---|---|---|
| $*$ | = | nondimensionalized |

Presented as Papers 98-4273, 98-4346, and 98-4347 at the AIAA Atmospheric Flight Mechanics Conference, Boston, MA, 10–12 August 1998; received 5 April 1999; revision received 8 December 1999; accepted for publication 21 June 2000. Copyright © 2000 by the authors. Published by the American Institute of Aeronautics and Astronautics, Inc., with permission.

*Research Engineer, Guided Missile Flight Performance Laboratory, First Division, Third Research Center, Technical Research and Development Institute, 1-2-10, Sakae, Tachikawa; currently Graduate Student, Tokyo Noko University, 2-24-16, Nakacho, Koganei, Tokyo 184-8588, Japan. Member AIAA.

†Research Engineer, Guided Missile Flight Performance Laboratory, First Division, Third Research Center, Technical Research and Development Institute, 1-2-10, Sakae, Tachikawa. Member AIAA.

‡Defense Systems Section No. 1, Defense Systems Department, 900, Fujiki, Tomioka. Member AIAA.

§Missile Project Engineering Department, 1, Kawasaki, Kakamigahara. Member AIAA.

## Introduction

ONE method of missile attitude control in use is the sidejet, which has rapid responses because it burns out in an instant (several milliseconds). When the side thruster equipped to the flying missile burns in the air, the flowfield becomes complicated. There are interactions between the sidejet and the supersonic external flow. It is known that the side force level due to the thruster changes when compared with the thruster in a vacuum. (A sketch of the flowfield is shown in Fig. 1.)

When the sidejet is exhausted perpendicular to the body axis at the forebody of the missile, the jet is bent downstream by the supersonic external flow and interacts with the fuselage and tail fins. A high-pressure area appears in front of the thruster nozzle, and a low-pressure area appears behind the nozzle. Considering forces and moments acting on the whole missile, those of aerodynamic interaction effects are produced by the influences of the high-pressure and low-pressure areas, except that of the jet thrust.

From previous works, with regard to aerodynamic interaction effects, the jet thrust varies with pressure ratio.[1] But the magnitude and extent of the interaction effects are not sufficiently investigated. It is shown that sidejet injection at the forebody of the rocket body decreases its thrust from 20 to 40%, including the tail fin interaction.[2]

Also, the pressure distribution and the forces with the aerodynamic interaction were measured in wind tunnels as the jet was injected into the external flow steadily.[3–5] Recently, computational fluid dynamics (CFD) analyses have been possible due to the progress of the numerical computation.[6] CFD predictions were compared to wind-tunnel test results.[7]

## Purpose of This Study

The purpose of this study is to conduct quantitative and qualitative estimations of sidejet aerodynamic interaction effects of a missile. This includes the following three effects: 1) complicated pressure distribution near the sidejet nozzle, 2) sidejet interactions with the missile body, and 3) sidejet interactions with the tail fins.

To achieve this, the sidejet aerodynamic interaction effects of the forces and moments were estimated quantitatively from wind-tunnel tests and CFD analyses. Actual effects were calculated from measured data in the flight tests, and the estimation method was validated by comparison with the data. Because the missile in this study was designed to have small tail fins and a long separation between the thrusters and the tail fins, there were few sidejet interactions with the aftbody and tail fins with angles of attack less than approximately 5 deg. This design was validated in cold-gas wind-tunnel tests using a whole missile body.

The estimation method is the combination of the wind-tunnel tests and the CFD analyses. It was conducted paying attention to the

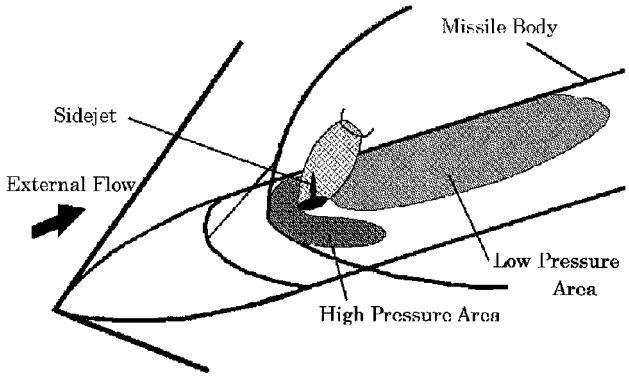


**Fig. 1 Sketch of the flowfield.**

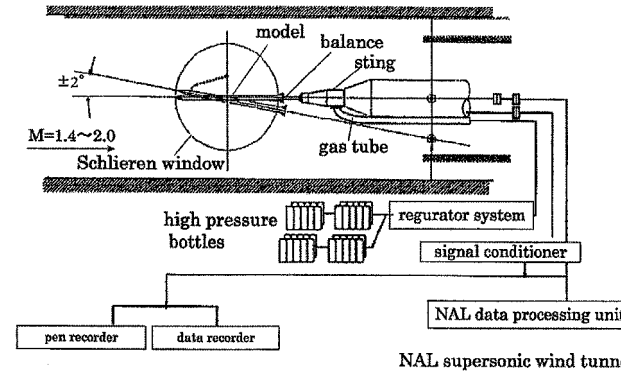


**Fig. 2 Outline of cold-gas wind-tunnel tests.**

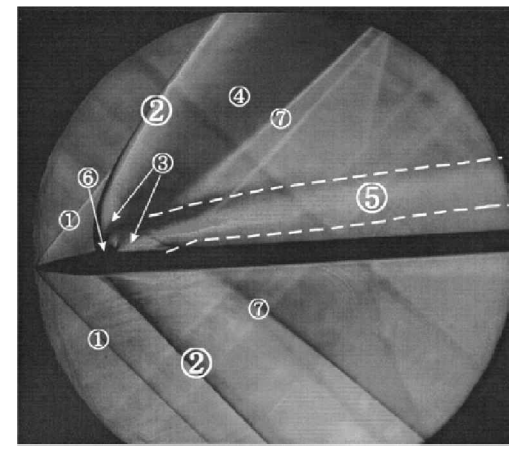


**Fig. 3 Schlieren photograph (vicinity of the sidejet): 1, oblique shock; 2, bow shock; 3, barrel shock; 4, expansion region; 5, jet path; 6, λ shock; and 7, recompression shock.**

unsteadiness of sidejet aerodynamic interaction effects that appear near the thruster nozzle and produce pressure differences on the missile surface. The outline of this method is shown later.

Forces and moments that are generated within several milliseconds of the thruster burn cannot be measured by current wind-tunnel testing techniques. It is difficult to estimate the sidejet aerodynamic interaction effects from the results of hot-gas wind-tunnel tests that correspond to the phenomena on the actual missile.

At first, to grasp sidejet aerodynamic interaction effects on the whole missile body, we conducted cold-gas wind-tunnel tests in which steady nitrogen gas was exhausted as the sidejet.

Next, wind-tunnel tests and CFD analyses were conducted using only the forebody model near the thrusters because the pressure distributions on the surface close to the thrusters induced aerodynamic interaction effects. However, the surface pressure on the aftbody of the missile does not vary when the thruster burns.

Two different types of wind-tunnel tests were conducted. One was the cold-gas test, and the other was the hot-gas test. In these tests, an impulsive solid propellant that has a very rapid burnout time (about 1.5 ms) was used to simulate the unsteady jet. In each test run, the surface static pressure distributions near the sidejet nozzle (hereafter called *external pressure*) were measured to describe the sidejet aerodynamic interaction effects. In the cold-gas tests, six components of the forces and moments were also measured to relate the external pressure distributions to the interaction forces and moments. The results of the hot-gas tests were compared with those of the cold-gas tests and the CFD analyses by using Navier–Stokes codes.

Finally, a similarity rule was derived by using the nondimensional expression of the external pressure distribution, and a new engineering estimation method was proposed for predicting the aerodynamic interaction forces and moments before conducting flight tests.

## Estimation Method of Sidejet Aerodynamic Interaction Effects

Shown here are the methods and results of the cold-gas tests using the whole-missile-body model and those of the cold-gas tests, hot-gas tests, and CFD analyses using forebody models near the thruster nozzle. The estimation method of sidejet aerodynamic interaction effects will be described at the end of the section.

Though sidejet aerodynamic interaction effects are unsteady phenomena that occur within several milliseconds, they were considered to be quasi-steady phenomena in the cold-gas tests. Because we assumed the interaction effects to be a temporal accumulation of forces and moments in steady phenomena within a very short time, the continuous jet was used.

### Cold Gas Tests Using the Whole-Missile-Body Model

*Testing Method*

The outline of the wind-tunnel tests is shown in Fig. 2. Tests were conducted in the transonic wind tunnel at Kawasaki Heavy Industries at $M = 1.4$ and the supersonic wind tunnel at the National Aerospace Laboratory with Mach number 1.4–2.0.

In these tests, the normal force and pitching moment were mainly measured while the jet was exhausted continuously from the nozzle both with and without external supersonic flow. Thruster chamber pressure was also measured. High-pressure nitrogen gas was supplied from high-pressure gas bottles and regulated to a fixed pressure. Then it was led through the sting, the hollow balance, and chamber and exhausted perpendicular to the model body axis. The scale of the test model is 24%.

*Results*

The schlieren photograph (Fig. 3) shows the bow shock upstream of the sidejet nozzle, the shock generated by the recompression of the external flow downstream of the jet, the jet path, and so on. Judging from the jet path, there were few interaction effects between the jet and tail fins of the missile.

At high angles of attack, there were sidejet interaction effects with the aftbody and tail fins. But, in the flight tests, measured data were with no or low angle of attack. Hereafter we pay attention to the forebody of the missile and continue analyzing the effects that appear near the thruster nozzle.

### Cold-Gas Tests Using the Forebody Model

*Testing Method*

To analyze the aerodynamic interaction effects, a series of wind-tunnel tests was run in the high-speed wind tunnel (vacuum-suction type). The pressure distribution and components of the forces and moments were measured near the sidejet nozzle.

Measurements were carried out separately using different models designed for the pressure distribution and for the forces and moments. A high-pressure gas supply unit prepared high-pressure nitrogen gas. Set at a specified pressure level, the gas was fed to the sidejet nozzle under steady-state conditions. For the model used to measure the six components of the forces and moments, both the nitrogen gas supply tube and the gas ejection nozzle were fixed to a sting to prevent the tube and the nozzle from contacting the forebody. This configuration avoided the erroneous detection of thrust generated by the jet via the balance mounted to the forebody of the model. The testing parameters were Mach number (0.5, 1.4, 2.0, 3.0, and 4.0), angle of attack (ranging from −10 to +10 deg), gas

supply pressure (from about $5 \times 10^6$ to about $6 \times 10^6$ N/m$^2$), and jet nozzle configurations.

*Results*

The static pressure distributions near the thruster nozzle are shown in Fig. 4. The greater the amount of sidejet gas exhausted, the larger the volume of external flow gas that was blocked. Therefore, it was found that the high-pressure area of the upstream shown in Fig. 1 became larger.

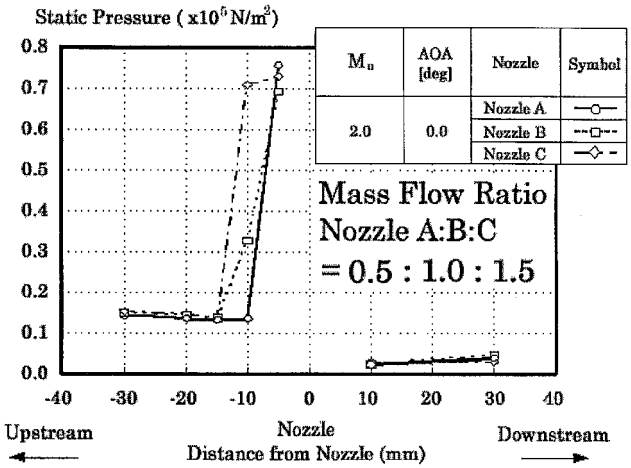


**Fig. 4 Static pressure distribution near the jet nozzle.**

**Hot-Gas Wind-Tunnel Tests**

*Testing Method*

The thrusters which were equipped in the missiles used in flight tests burn out in an instant (about 1.5 ms a thruster). To simulate this phenomenon, a propellant used in actual flight tests was employed in the wind-tunnel test as a sidejet gas supply source. The operating parameters of the sidejet gas were set to be the same as those in the flight tests to provide a similar thruster burning pressure profile. The burnout time, the jet specific heat ratio, and maximum burning pressure were 1.5 ms, 1.14, and about $1.5 \times 10^8$ N/m$^2$, respectively.

The external pressures near the sidejet nozzle were measured in a hypersonic wind tunnel (intermittent blowdown type). In this test, the uniform flow Mach number and the static pressure were set to 2.0 and $1.0 \times 10^5$ N/m$^2$, respectively. A jet nozzle configuration that was similar to that used in the actual flight tests was selected. The outline of these tests is shown in Fig. 5.

*Results*

Figures 6 and 7 show some of the results. Figure 6 shows that, in response to an abrupt increase followed by a decrease in the thruster chamber pressure, the external pressure distribution in front of the sidejet nozzle also increased and then decreased concurrently. It is also found that there is a time lag between the time histories of the thruster chamber pressure and those of the external pressure. Figure 7 shows schlieren photographs taken by a high-speed video camera (2000 frames/s). As in Fig. 3, a bow shock appears at the upstream of the thruster nozzle, quantitatively indicating the existence

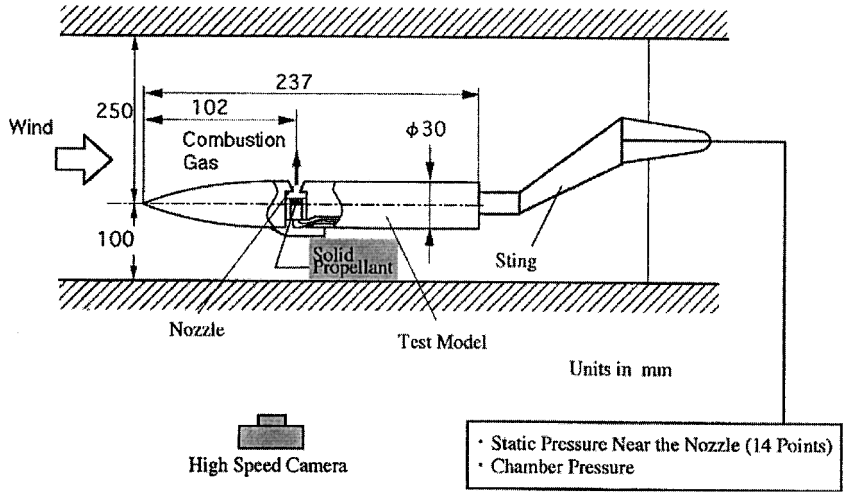


**Fig. 5 Outline of hot-gas tests.**

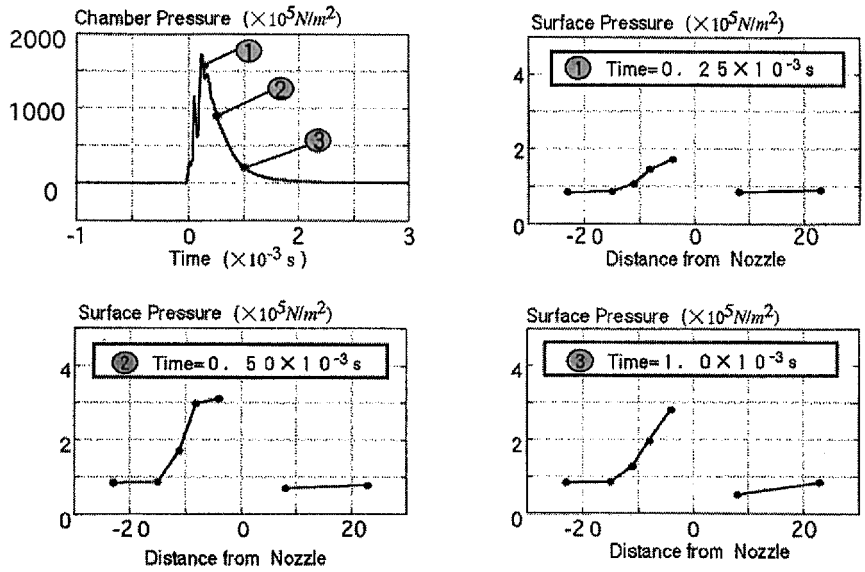


**Fig. 6 Chamber pressure and static pressure in hot-gas tests.**

of phenomena similar to that obtained in the cold-gas wind-tunnel tests.

**CFD Analyses**

CFD analyses were conducted in the same conditions as those of the cold-gas tests. Three-dimensional Navier–Stokes codes that could simulate the shock-boundary-layer phenomena were used, which significantly affects sidejet aerodynamic interaction effects. We estimated inviscid terms with a second-order MUSCL upwind TVD scheme and viscous ones with a central difference method and Baldwin–Lomax turbulence model. The computational grids were dense in the vicinity of the sidejet nozzle and on the model body surface. The number of grid points was about 195,000.

The results confirm that CFD computational results validated those of the cold-gas tests. Figures 8 and 9 show comparisons of oil flows and pressure distributions near the thruster nozzle, respectively. It was confirmed that CFD analyses simulated sidejet aerodynamic interaction effects quantitatively and qualitatively.

**Estimation of Sidejet Aerodynamic Interaction Effects**

We proposed a method for predicting sidejet aerodynamic interaction effects. A similarity rule was applied for the prediction, which uses the nondimensional expression of the pressure field that was based on the external pressure of the body surface near the thruster nozzle.

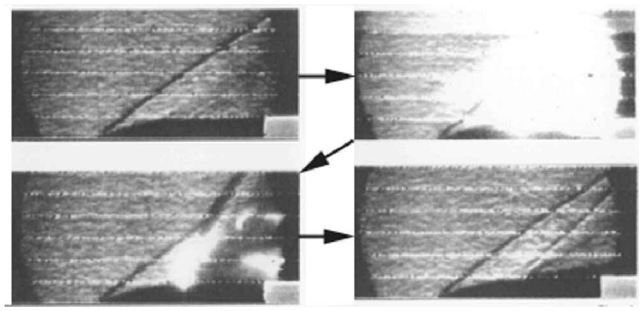

**Fig. 7 Schlieren photographs of hot-gas tests.**

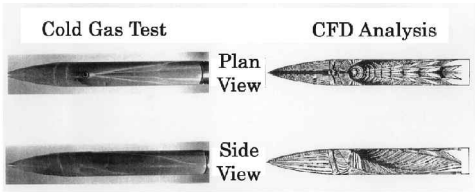


**Fig. 8 Comparison of cold-gas tests (oil flow) with CFD analyses.**

*Similarity Rule in the Pressure Field*

Aerodynamic interaction phenomena near the sidejet nozzle are complex. They depend significantly on the amount of interference of the jet blast with the external uniform flow. Aerodynamic interaction forces and moments on the missile are closely related to the maximum pressure $P_{\max}$ between the bow shock and the sidejet. If the interference height is assumed to be represented by the Mach disk height $h_j$, then a similarity rule among the results of the hot-gas and cold-gas wind-tunnel tests and the CFD analyses should be established by introducing nondimensional pressure $C_p^*$ and length $\ell^*$. The nondimensional expression of pressure and that of length are written as follows:

$$C_p^* = \frac{P - P_u}{P_{\max} - P_u} \tag{1}$$

$$\ell^* = \frac{\ell}{h_j} \tag{2}$$

where the Mach disk height was derived from the quasianalytical equations[8]

$$h_j = d_j \cdot M_j^{\frac{1}{4}} \left(\frac{P_{0j}}{P_u}\right)^{\frac{1}{2}} \left[\frac{g_2(M_j, \kappa_j)}{g_1(M_u, \kappa_u)}\right]^{\frac{1}{2}} \tag{3}$$

$$g_1(M_u, \kappa_u) = \frac{2}{3}\left(1 + \frac{\kappa_u - 1}{2} M_u^2\right)^{\kappa_u/(\kappa_u - 1)} \times \left(\frac{2\kappa_u}{\kappa_u + 1} M_u^2 - \frac{\kappa_u - 1}{\kappa_u + 1}\right)^{-1/(\kappa_u - 1)} \times \left\{\frac{1 + (\kappa_u - 1)M_u^2/2}{(\kappa_u + 1)M_u^2/2}\right\}^{-\kappa_u/(\kappa_u - 1)}$$

$$g_2(M_j, \kappa_j) = M_j \left[\frac{2}{\kappa_j + 1}\left(1 + \frac{\kappa_j - 1}{2} M_j^2\right)\right]^{(\kappa_j + 1)/2(1 - \kappa_j)} \times \left(\frac{\kappa_j + 1}{2}\right)^{-\kappa_j/(\kappa_j - 1)}$$

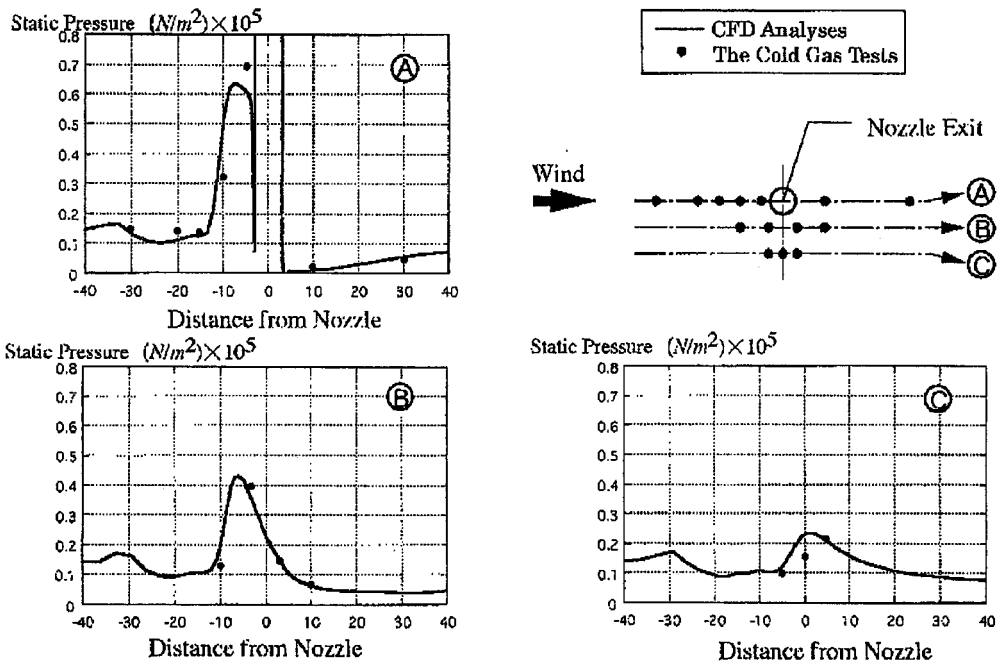


**Fig. 9 Comparison of cold-gas tests with CFD analyses (pressure distribution near the thruster nozzle).**

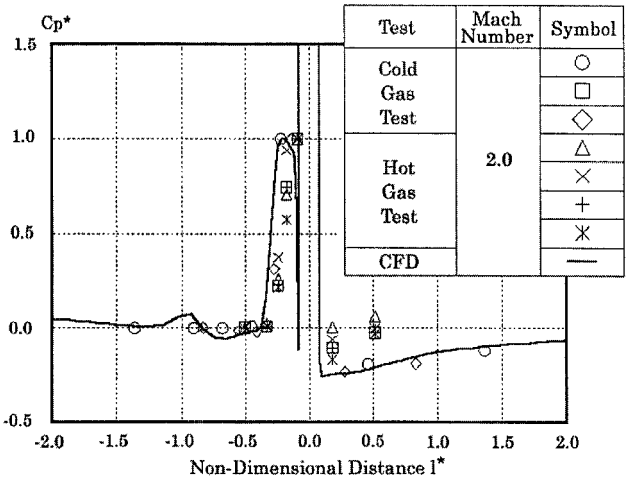


**Fig. 10 Nondimensional pressure distributions of cold-gas and hot-gas wind-tunnel tests and CFD analyses.**

These equations are valid in steady conditions. But when we used them in the cold-gas tests, we assumed unsteady phenomena to be steady ones in a very short time. Because the flowfield in unsteady conditions was similar to that in steady conditions, we treated unsteady data in the hot-gas tests as steady ones.

By using these nondimensional expressions, data of steady cold-gas tests, unsteady hot-gas tests, and steady CFD analyses were plotted on the same figure. The similarity of phenomena was verified from Fig. 10.

*Estimation Method*

Aerodynamic forces and moments on the flying missile are determined by the integration of the body surface pressure distributions over the body surfaces as follows:

$$\boldsymbol{F} = \iint_S (P - P_u)\,\mathrm{d}\boldsymbol{S} = (P_{\max} - P_u)h_j^2 I_{\mathrm{CPF}} \tag{4}$$

$$I_{\mathrm{CPF}} = \iint_{S/h_j^2} C_p^*\,\mathrm{d}\frac{\boldsymbol{S}}{h_j^2} \tag{5}$$

$$\begin{aligned}\boldsymbol{M} &= \iint_S (P - P_u)(\ell - l)\,\mathrm{d}\boldsymbol{S} \\ &= \iint_S (P - P_u)\ell\,\mathrm{d}\boldsymbol{S} - l\iint_S (P - P_u)\,\mathrm{d}\boldsymbol{S} \\ &= (P_{\max} - P_u)h_j^3 I_{\mathrm{CPM}} - \boldsymbol{F}\cdot l\end{aligned} \tag{6}$$

$$I_{\mathrm{CPM}} = \iint_{S/h_j^2} C_p^*\ell^*\,\mathrm{d}\frac{\boldsymbol{S}}{h_j^2} \tag{7}$$

where $I_{\mathrm{CPF}}$ and $I_{\mathrm{CPM}}$ were derived from CFD analyses of sidejet aerodynamic interaction effects in the steady state and $h_j$ was calculated from Eq. (3).

From these analyses, the characteristics of sidejet aerodynamic interaction effects were observed for unsteady phenomena near the thruster nozzle and the production of aerodynamic interaction effects caused by the pressure distribution difference. It is especially important to notice that the hot-gas-test results, which used the same propellant equipped in the actual flight test missiles, show the unsteadiness of the phenomena. The cold-gas tests and the CFD analyses using a steady continuous jet are effective and valid for the estimation.

## Calculation from Flight Test Results

**Outline of Missile**

The missiles used in the flight tests were manufactured to confirm the thruster attitude controls and to measure sidejet aerodynamic interaction effects in flight conditions.

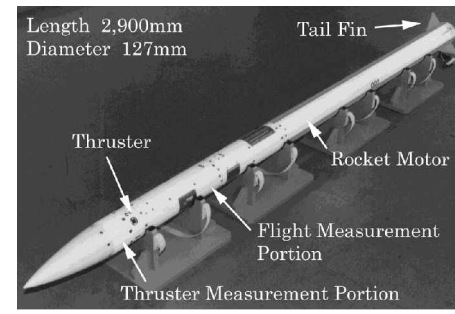


**Fig. 11 Photograph of the missile.**

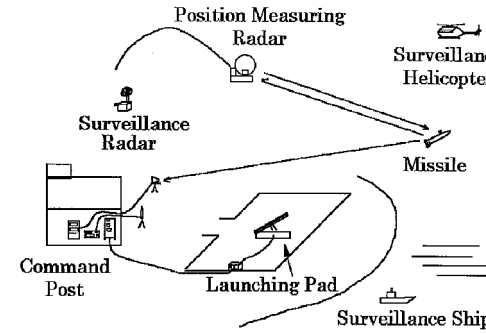


**Fig. 12 Measuring environment of flight test.**

The missile consists of the head cover, the thruster measurement portion, the flight measurement portion, the rocket motor, and the tail fins. The sidejet of the missiles was achieved by small-size solid propellant rocket motors whose impulse was about 5 N · s. The burnout time is 1.5 ms. The thruster measurement portion has four impulsive side thrusters and measures very rapid phenomena near the thruster when the thruster is burning. The flight measurement portion controls the timing when the thruster begins to burn and measures flight data. The rocket motor thrust is about 19,000 N. The tail fins have some constant angle to the $x$ body axis so the missile rolls while flying and can control the attitudes around pitch and yaw axes. A photograph of the missile is shown in Fig. 11.

**Test Method**

The flight tests were implemented at the Niijima test center, Technical Research and Development Institute, Japan Defense Agency, in October 1996. The missile was launched from the launching pad on the ground at the launching angle of 25 deg. The burnout time of the rocket motor was about 1.6 s, and the maximum velocity of the missile was about $M = 2.3$. After the rocket motor had burned out, four side thrusters burned according to the preprogrammed sequence in the following two modes.

Mode 1: The side thrusters burn consecutively to the same direction based on the earth coordinates.

Mode 2: The side thrusters burn to preprogrammed directions having long-enough time intervals based on the earth coordinates.

In mode 1, the data of the flight-path angle change were mainly measured to obtain flight-path-angle controllability using side thrusters. In mode 2, single-thruster performances were mainly obtained to grasp dynamic responses and structural characteristics of the missile. The telemeter transmitted the measured signals obtained in flight. The position-measuring radar was used to obtain position data of the missile. Also, characteristics of the missile launching were measured optically by high-speed cameras and video recorders on the ground and from a surveillance helicopter. The measuring environment of the flight test is shown in Fig. 12.

During the flight tests, accelerations and angular velocities of the missile body were measured. Impulsive accelerations, impulsive angular velocities, thruster burning pressures, external pressures near the thruster nozzle, and other parameters were measured in the thruster measurement portion when the thruster was burning.

**Data Reduction Methods**

The flight-path angle and quantity of sidejet aerodynamic interaction effects on the forces and moments were calculated from measured data of accelerations, angular velocities, and thruster impulse in the flight tests. These equations were derived from the transfer functions of equations of motion of a body in which the Laplace final value theorem was applied. They are expressed as follows:

$$\Delta\gamma = \left[\left(1+\frac{\Delta \boldsymbol{F}}{\boldsymbol{F}}\right)+\left(1+\frac{\Delta \boldsymbol{M}}{\boldsymbol{M}}\right)\frac{l}{\mathrm{SSM}}\right]\cdot\frac{I_0}{mV}$$

$$\Delta q = \frac{I_0\cdot l}{I_y}\cdot\left(1+\frac{\Delta \boldsymbol{M}}{\boldsymbol{M}}\right) \tag{8}$$

**Flight Test Results**

Flight tests of four missiles were successfully conducted. Necessary data were obtained to estimate sidejet aerodynamic interaction effects of the forces and moments acting on the missile. A photograph of the missile launched from the launching pad was taken by a camera near the launching pad and is shown in Fig. 13.

Static pressures near the thruster nozzle, thruster burning pressures, impulsive accelerations, and impulsive angular velocities when the thruster was burning were obtained. These data showed that very rapid phenomena occurred while the thruster was burning. Examples are shown in Figs. 14–17.

Figure 14 shows that a high-pressure and a low-pressure area appeared upstream and downstream of the thruster nozzle as shown in Fig. 1. Figure 15 shows delay time and burnout time of the thruster to be about 0.5 and 2 ms, respectively. When the thruster was burning in the positive $y$ direction, Fig. 16 shows the duration and direction of impulsive accelerations to be almost the same as those when the thruster is burning. Figure 17 shows the impulsive angular velocity to the yaw direction. This corresponds to the rotational direction. By inspecting Figs. 14, 16, and 17, we compared the forces and moments that the thruster itself produced with those of the difference of the external pressure distribution induced by interaction effects. The amount of the former is bigger than that of the latter, but the duration time of the phenomena is smaller. So, from 1.0 to 2.0 ms after the combustion of the thruster burn, it was found that angular velocity was measured to the opposite direction corresponding to the opposite yaw direction of the impulsive acceleration.

Accelerations and angular velocities on the whole missile body were obtained. The examples of accelerations and angular velocities are shown in Figs. 18 and 19, respectively. These data were obtained

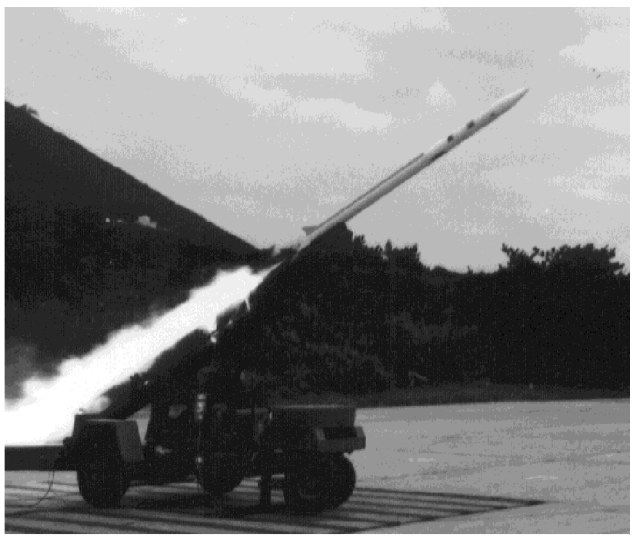

**Fig. 13 Photograph of the missile launched from launching pad.**

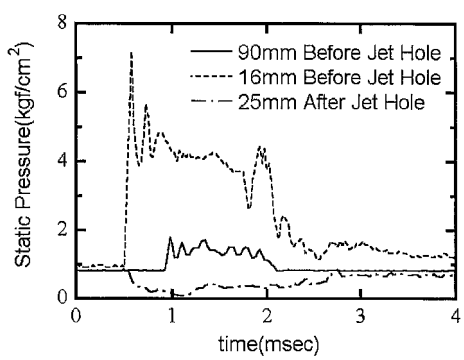


**Fig. 14 Static pressure near the jet nozzle.**

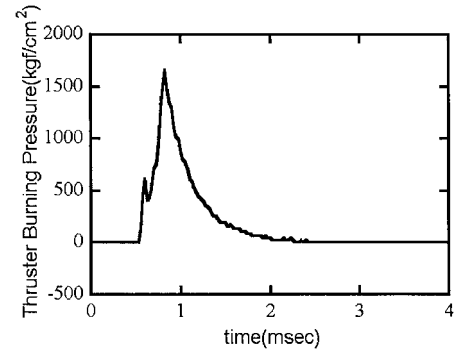


**Fig. 15 Thruster burning pressure.**

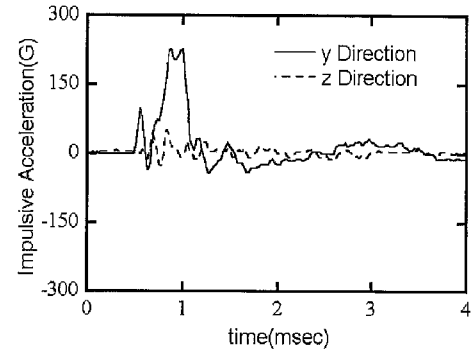


**Fig. 16 Impulsive acceleration.**

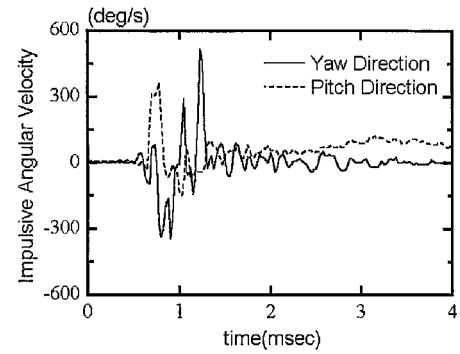


**Fig. 17 Impulsive angular velocity.**

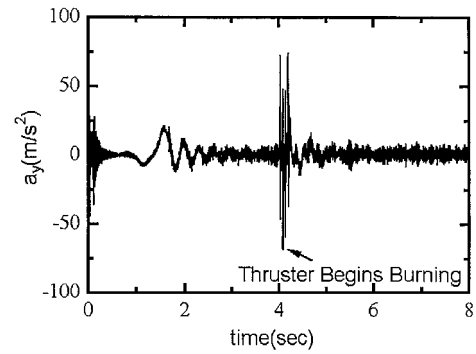


**Fig. 18 Acceleration.**

**Table 1 Aerodynamic interaction effects**

| Value | $\Delta F/F$, % | $\Delta M/M$, % |
|---|---|---|
| Estimated | −12 | −14 |
| Flight Test | −10 | −10 |

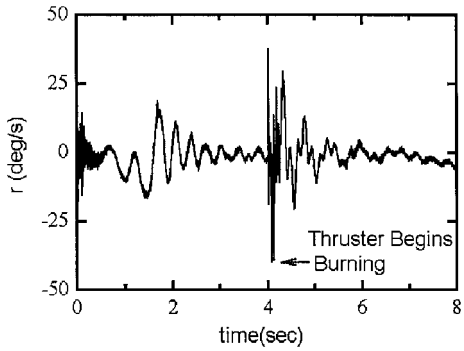


**Fig. 19 Angular velocity.**

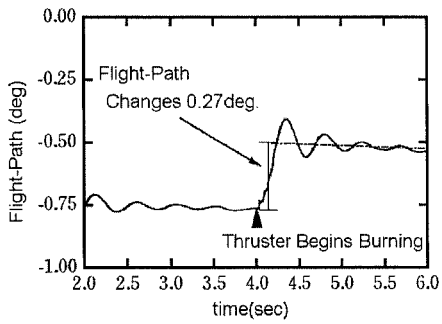


**Fig. 20 Change of the flight-path angle. Because a cross wind was blowing in the flight test, the flight-path angle changed constantly to a negative direction.**

in the missile body axes. Because the missile rolled while flying, the accelerations of the thruster occurred in different directions in the missile body axis. But it was confirmed that thrusters burned to almost the same direction in the fixed-ground coordinates.

Next the flight-path angle and the velocity of the missile were calculated from these data. The example of the flight-path angle change in mode 1 when the thrusters burned is shown in Fig. 20. After four thrusters finished burning to almost the same direction within 0.3 s, the flight-path angle changed 0.27 deg and the attitude control performed successfully. The velocities of the missile were $M = 1.8$ in mode 1 and between 1.7 and 2.1 in mode 2 when the thruster burned at the flight tests.

## Comparison Between Estimated and Measured Results

### Estimation Method

Sidejet aerodynamic interaction effects were estimated from Eqs. (4) and (6) derived from the similarity rules in the pressure field. $I_{CPF}$ and $I_{CPM}$ expressed in Eqs. (5) and (7) were calculated from the results of the CFD analyses, and others were estimated from the wind-tunnel tests.

The estimated values of sidejet aerodynamic interaction effects of the force $\Delta F/F$ and the moment $\Delta M/M$ from the similarity rules in pressure field were about −12 and −14%, respectively.

### Flight Test Results

Sidejet aerodynamic interaction effects of the force and moment are both −10%, calculated from the acceleration, the angular velocity, the flight-path angle change, and so on in the flight tests using Eqs. (8). These results are summarized in Table 1.

## Conclusions

Wind-tunnel tests, CFD analyses, and flight tests were conducted to investigate aerodynamic interaction effects between the sidejet and the external supersonic flow. The conclusions are as follows:

1) The databases of sidejet aerodynamic interaction effects of the missile were obtained from the cold-gas and the hot-gas tests. Aerodynamic interaction effects were estimated from the pressure distribution near the thruster nozzle, and the validity of the CFD analyses was confirmed.

2) The results of wind-tunnel tests and CFD analyses were summarized by using nondimensional expressions of pressure and length, and a method to estimate sidejet aerodynamic interaction effects from the similarity rule in the pressure field was proposed. Next this method was applied to the flight tests.

3) Aerodynamic interaction effects from the flight test results have good agreement with the estimation method mentioned. It is confirmed that this approach is very effective to estimate sidejet aerodynamic interaction effects.

Consequently, robust databases and estimation methods of sidejet aerodynamic interaction effects, which would be helpful to design a missile employing the use of sidejets, were obtained.

## Acknowledgments

The authors acknowledge the following people for their support: S. Takanashi and A. Yoshida (Technical Research and Development Institute, Japan Defense Agency) for their advice in conducting this study, T. Yamanaka and N. Sekino (IHI Aerospace Co., Ltd.) for manufacturing the thruster measurement portion and for analyses using forebody model, and H. Tokunaga (Kawasaki Heavy Industries, Ltd.) for manufacturing the flight measurement portion and for analyses using the whole-missile-body model.

## References

[1] Janos, J., "Loads Induced on a Flat-Plate Wing by an Air Jet Exhausting Perpendicularly Through the Wing and Normal to a Free-Stream Flow of Mach Number 2.0," NASA TN D-649, 1961.

[2] Hashidate, M., and Shimizu, F., "Experimental Investigation of the Effect of Side Jet on a Tailfin of a Rocket in Supersonic Flow," National Aerospace Laboratory, NAL TR-480, Tokyo, 1985 (in Japanese).

[3] Spaid, F., and Zukoski, E., "A Study of the Interaction of Gaseous Jets from Transverse Slots with Supersonic External Flows," *AIAA Journal*, Vol. 6, No. 2, 1968, pp. 205–212.

[4] Chambers, R., and Collins, D., "Stagnation Temperature and Molecular Weight Effects in Jet Interaction," *AIAA Journal*, Vol. 8, No. 2, 1970, pp. 287–293.

[5] Brandeis, J., and Gill, J., "Experimental Investigation of Side-Jet Steering for Supersonic and Hypersonic Missiles," *Journal of Spacecraft and Rockets*, Vol. 33, No. 3, 1996, pp. 346–352.

[6] Ward, S., "A Computational Model for the Performance of Jet-Interaction Steering Control Systems for Conical Missiles," AIAA Paper 87-0069, 1987.

[7] Shang, J., McMaster, D., Seaggs, N., and Buck, M., "Interaction of Jet in Hypersonic Cross Stream," *AIAA Journal*, Vol. 27, No. 3, 1989, pp. 323–329.

[8] Billing, F., Orth, R., and Lasky, M., "A Unified Analysis of Gaseous Jet Penetration," *AIAA Journal*, Vol. 9, No. 6, 1971, pp. 1048–1058.

J. P. Gore
*Associate Editor*